Analysis of a scaled stone masonry façade subjected to differential settlements

G. Giardina[1], A. Marini [2], P. Riva,[2]and E. Giuriani [3]

ABSTRACT

Historical masonry structures are vulnerable to differential settlements of the ground. This vulnerability is potentially higher for historic buildings on wooden pile foundations, which can have their bearing capacity reduced by material deterioration. In order to protect such buildings from the effect of soil subsidence it is therefore essential assessing their response to settlements. The aim of this paper is to investigate the settlement-induced damage on a stone masonry façade. For the first time, experimental testing and computational analyses were performed on a scaled model of a specific existing historic structure, the Loggia palace in Brescia, Italy. Differential settlements were applied to dry blocks and mortar joints models of the façade. Experimental results showed the capability of the façade to reach a new equilibrium configuration following the subsidence of two adjacent columns. This approach can be used to assess the behaviour of similar structures. The validated numerical model confirms the interpretation of the failure mechanism and has the potential to allow extending the approach to a wider range of settlement and structural scenarios, as well as to different buildings.

Keywords: cracking; damage assessment; differential settlements; experimental testing; physical modelling; masonry; numerical modelling

INTRODUCTION

The vast majority of historic buildings is made of unreinforced masonry, which typically exhibits a quasi-brittle response to ground movements. Masonry structures are therefore vulnerable to different sources of differential settlements, like water pumping (Meli and Sanchez-Ramirez, 1997; Ovando-Shelley et al., 2007), underground excavations (Burland et al., 2001), tunnelling-induced vibrations (New, 1990), mining (de Vent, 2016), earthquakes (D'Ayala, 2013).

Historic buildings on soft soil have been often supported by wooden pile foundations, which may entail an additional source of vulnerability for the structure.

---

[1]Department of Architecture and Engineering, University of Bath

[2]Department of Engineering and Applied Sciences, University of Bergamo

[3]Department of Civil Engineering, Architecture, Land and Environment, University of Brescia

In case of buildings adjacent to tunnelling, pile foundations may lead to the transmission of larger settlements to the structure, if compared to shallow foundations (Jacobsz et al., 2006; Korff and Mair, 2013; Franza and Marshall, 2018). Furthermore, wooden foundations are subjected to the aggression of bacteria in anoxic conditions and to fungal attack when exposed to oxygen (van de Kuilen, 2007; Clausen, 2010; Klaassen and Creemers, 2012). Due to ground water level variations, wooden piles can therefore deteriorate and have their bearing capacity significantly reduced or totally vanished. This can in turn lead to progressive or sudden change in load transfer between the building and therefore to building deformations and structural damage (Bettiol et al., 2016). In the absence of a systematic survey on the current conditions of wooden foundations in urban areas, assessing the response of historic structures to potential settlements is vital for the protection of architectural heritage.

Simplified procedures are available to address the damage assessment of a large number of buildings in the proximity of construction sites (Burland and Wroth, 1974; Burland et al., 1977; Boscardin and Cording, 1989; Burland, 1995; Mair et al., 1996; Potts and Addenbrooke, 1997; Son and Cording, 2005; Franzius et al., 2006a; Goh and Mair, 2011; Dalgic et al., 2018b). For those buildings considered at risk after the initial screening, numerical models have been developed to include the effect of complex building geometries (Burd et al., 2000; Franzius et al., 2006b; Giardina et al., 2010; Losacco et al., 2014), large openings (Son and Cording, 2007; Pickhaver et al., 2010; Giardina et al., 2015b), building weight (Burd et al., 2000; Liu et al., 2000; Franzius et al., 2004; Rampello et al., 2012; Giardina et al., 2015c,a), initial structural damage (Giardina et al., 2015c; Dalgic et al., 2018a), nonlinear response of the soil (Burd et al., 2000; Liu et al., 2000; Franzius et al., 2006b), nonlinear behaviour of the building material (Boonpichetvong and Rots, 2005; Son and Cording, 2005; DeJong et al., 2008; Giardina, 2013; Amorosi et al., 2014), soil-structure interaction (Son and Cording, 2005; Franzius et al., 2006a; Giardina et al., 2013). To make reliable predictions, numerical models need to be preliminarily validated by comparison with experimental results. However, up to date only few experiments of complex masonry structures subjected to settlements have been published (Son and Cording, 2005; Laefer et al., 2011; Giardina, 2013; Nghiem et al., 2014; Ritter et al., 2017a).

This paper aims at understanding the response of a masonry stone façade to differential settlements. It presents an experiment performed on a 1/20th scaled model of the main façade of an historical palace in the city of Brescia, Italy, subjected to foundation settlements caused by the degradation of wooden pile foundations. The model is representative of typical masonry façades of the Italian cultural heritage. Progressive vertical displacements were applied in cascade to two adjacent façade columns, in order to investigate the failure mechanism and quantify the prototype damage. Displacements and damage monitoring throughout the test enabled to correlate the imposed settlement with the façade deformation, damage pattern evolution and crack width opening rate. Different tests were performed to evaluate the effect of selected modelling assumptions on the

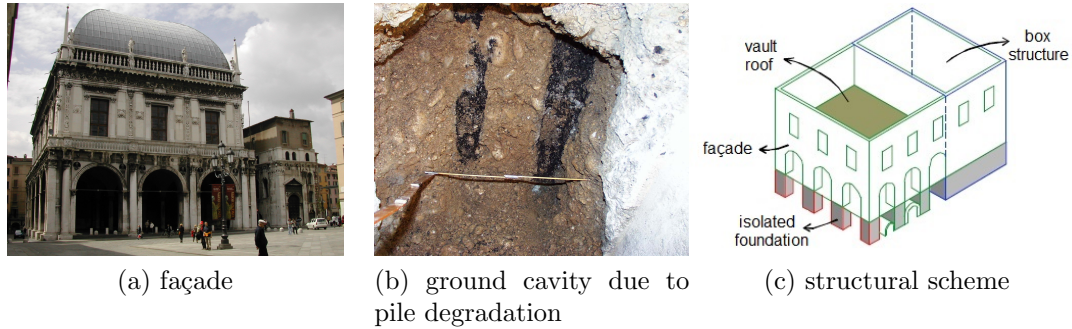| (a) façade | (b) ground cavity due to pile degradation | (c) structural scheme |

FIG. 1: Loggia Palace, Brescia, Italy.

structural response. First, the settlements were applied to a dry block model, to identify the qualitative crack pattern and failure mechanism. Second, the test was repeated on the same model with amplified vertical loads, to reproduce the stress conditions of the full scale façade and evaluate the scale effect on the final response. Finally, the differential settlement was applied to a façade model with mortar joints and amplified loading, to determine the influence of the mortar on the induced crack pattern. The experimental results were used to validate a finite element model of the tested structure; discrete and continuum cracking models were applied, to evaluate their ability to reproduce the façade nonlinear behaviour.

THE LOGGIA PALACE IN BRESCIA, ITALY

The Loggia Palace is an ancient stone masonry building on wooden pile foundations (Fig. 2a), built in the XIV century. In 1999, a field investigation revealed that the façade columns rest on isolated foundations, and that the compaction piles were heavily degraded (UNIBS, 1999). For most of the piles, only cavities of approximately 120 mm of diameter and 800 mm long were left, with a distribution of 12 to 16 cavity/m^2 (Fig. 2b). With this cavity density, in case of soil subsidence the foundation would settle of hundreds of millimetres, and a differential settlement of one of the columns, especially the corner ones, could cause severe structural damage and affect the palace global stability.

Such a scenario seriously concerned the local authorities, and was made more threatening by a similar prior case: in 1986 the church of S. Maria del Suffragio in Milan was severely damaged by a sudden localised subsidence that caused a significant settlement of the central column. This settlement triggered the cascade displacement of the adjacent columns and led to the severe damage of the supported arches. Given this precedent and the state of the Loggia foundations, an experimental test was designed prior to the construction of the city metro line, to assess the potential damage of the structure in case of differential settlements of its foundations.
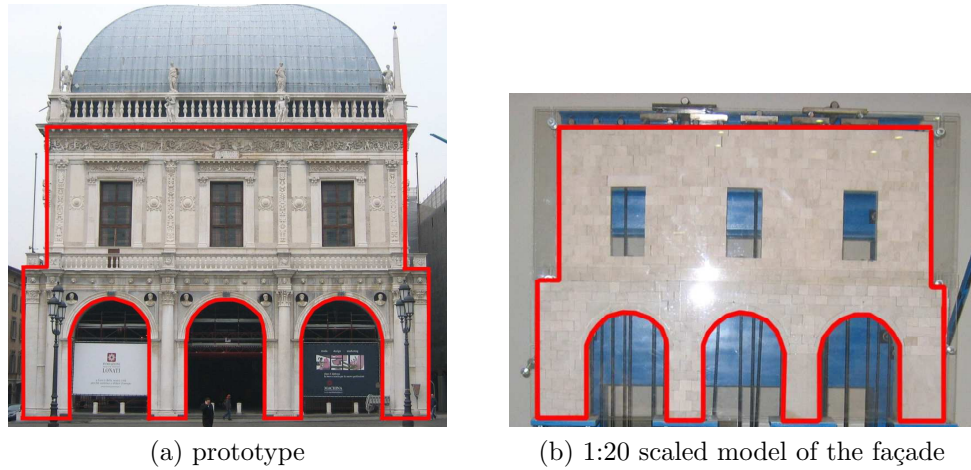
3

(a) prototype　　　　　　　　(b) 1:20 scaled model of the façade

FIG. 2: Loggia Palace physical modelling

EXPERIMENTAL SET-UP

This section describes the design of the experimental test, addressing the main modelling choices in terms of geometrical scaling, load amplification and monitoring procedures.

Model geometry

The tested scaled model reproduced the arched façade of the Loggia Palace (Fig. 2c), and it is representative of masonry façades on isolate foundations, which are particularly vulnerable to differential settlement. The 1/20th scaled model accurately reproduced the prototype geometry (Fig. 2). Only the structural components were modelled, while balustrades, mouldings and decoration elements were neglected. The façade was assembled in the laboratory of the University of Brescia using 705 blocks of Botticino Classic marble, the same material of the Loggia Palace. The 13 adopted block typologies were identical in shape and proportions to the prototype ones and therefore precisely replicated the original pattern of the façade covering blocks. This allowed for an accurate simulation of the settlement-induced damage mechanism. The model geometry is shown in Figure 3.

During their construction, the arches were supported by centring frames made of expanded polystyrene. The horizontality of the upper locks was guaranteed by small adjustments of the keystone element. In the dry block model, where necessary, putty layers were inserted between blocks to assure the full contact of the blocks and were isolated by pieces of cling-film, to avoid adhesion and reduce friction. Furthermore, the layers between adjacent blocks were cut vertically to avoid any additional internal constraint.

After the first two tests were performed on the dry block model, the structure was dismounted and the blocks were numbered to allow for the subsequent reassembling of the model with lime mortar joints. The marble blocks that had been damaged during the first tests were identified and replaced. 1/20th scaled
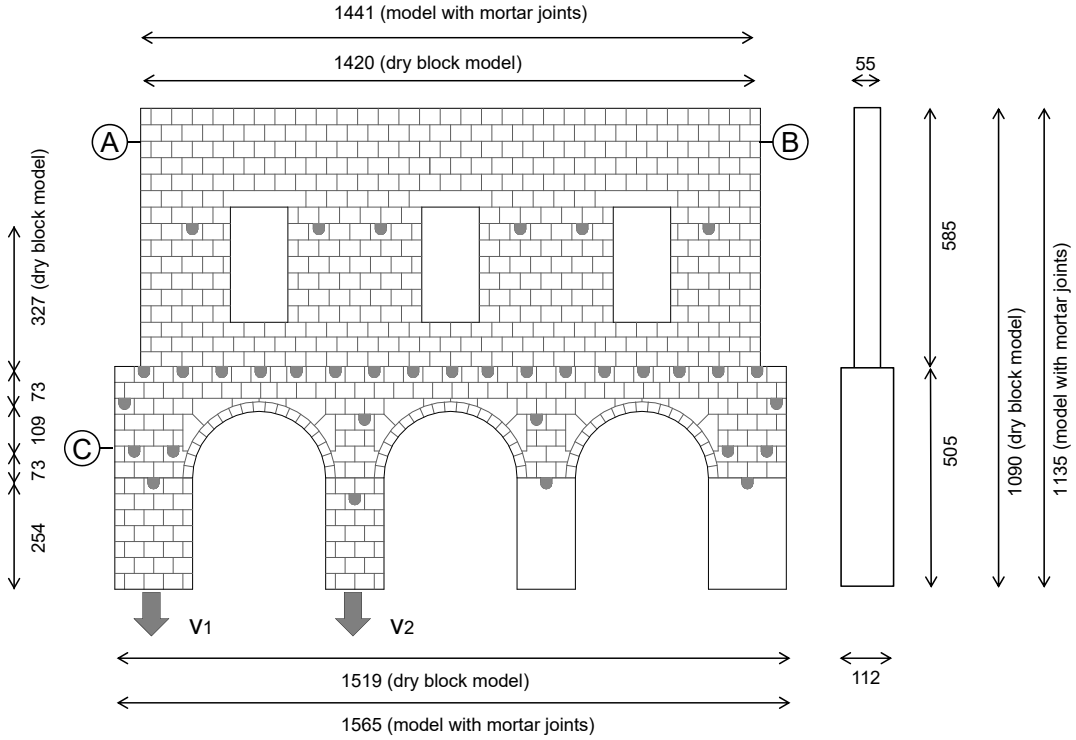
FIG. 3: Model dimensions (in mm), brick bond, location of amplified loads, applied displacements v_1 and v_2 and mechanical dial gauges a, b and c.

mortar layers of approximately 0.75 mm of thickness were inserted between the blocks of the new model. This increased the global dimensions of the model, as illustrated in Figure 3. In order to compensate for the different height between the two left columns, where mortar layers were added, and the two right columns, formed by a single marble block, a 10 mm thick metal plate was inserted at the base of each of the two right columns.

To achieve the façade verticality, a transparent Perspex sheet was located in front of the structure. Once the façade was built, the panel was moved 5 mm away from the structure to avoid any friction between the Perspex and the marble. The panel also served as a safety barrier during the test execution.

The test set-up consisted of a 3D steel frame with dimensions of $1.5 \times 2.3 \times 1$ m (Fig. 4a). The high stiffness of the steel frame guaranteed that possible frame deformations would be negligible with respect to the displacements monitored during the test. The four front frame stiles were surmounted by four rectangular plates, which directly support the façade columns. Each plate corner rested on a hexagonal nut, which was connected to a screw welded on the lower plate (Fig. 4b). This allowed for an accurate calibration of the plate height. For each nut complete turn, the imposed displacement was equal to the screw pitch, i.e. 2.5 mm.
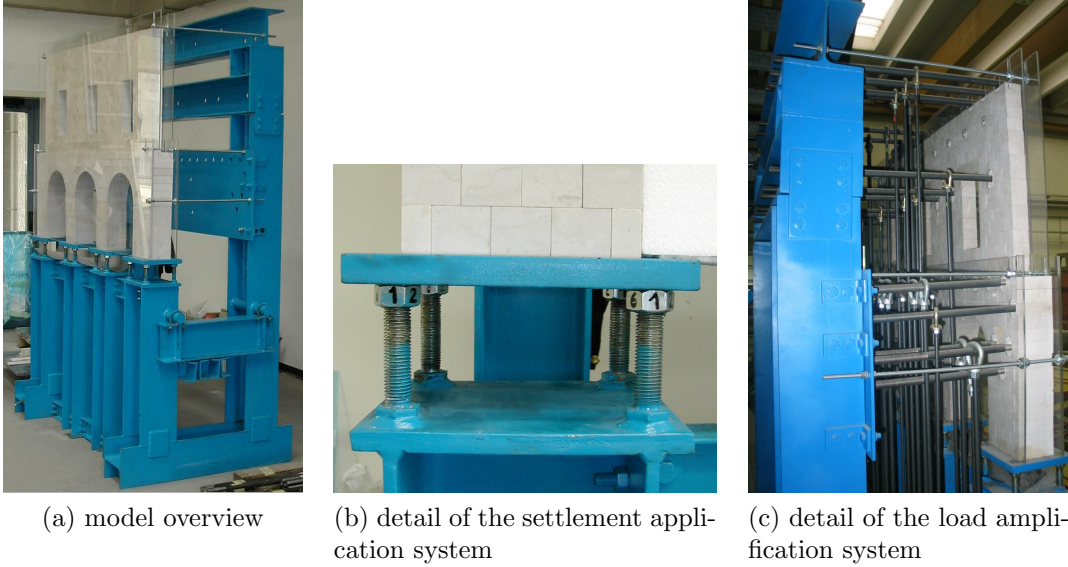
(a) model overview   (b) detail of the settlement application system   (c) detail of the load amplification system

FIG. 4: Experimental set-up

Loading system

To compensate for the reduced geometrical scale of the model and avoid problems of stress and strain, a dimensional analysis (Buckingham, 1914) was made. Accordingly, scaled factor of the load was obtained as follows:

$$K_F = K_E K_L^2 = K_\sigma K_L^2 = K_a K_L^2 = K_\gamma K_L^3 \tag{1}$$

where K_F is the point load scale factor, K_E is the Young's modulus scale factor, K_L is the length scale factor, K_σ is the stress scale factor and K_γ is the specific weight scale factor. Since the aim of the experiment was to reproduce the prototype stress conditions in the scaled model, $K_\sigma = 1$. The choice of using for the model the same material of the actual palace led to the condition $K_E = 1$. Since the geometrical factor $K_L = 1/20$, Equation 1 yields $K_F = 1/400$ and $K_\gamma = 20$.

Because the material selection imposed $K_\gamma = 1$ and excluding the use of a geotechnical centrifuge to induce an amplified acceleration to the structure (Ritter et al., 2017b), the loads acting on the model were amplified to reproduce the real stresses. The extra load was applied at 43 discrete points through a system of vertical and horizontal bars (Figs. 4c and 5). Each horizontal bar transferred the load imposed by the vertical bar to the façade

The horizontal bars were placed on different levels to optimise the available space usage (Fig. 4c). The upper bars, which transmitted the prototype roof weight to the model, rested directly on top of the façade. The number of required bars was reduced by using load distribution devices. To reduce their axial stiffness, the vertical bars were connected to the fixed frames by a series of cup springs. The characteristic non-linear load-displacement relationship of the springs allowed to measure the force applied to the bar through the spring
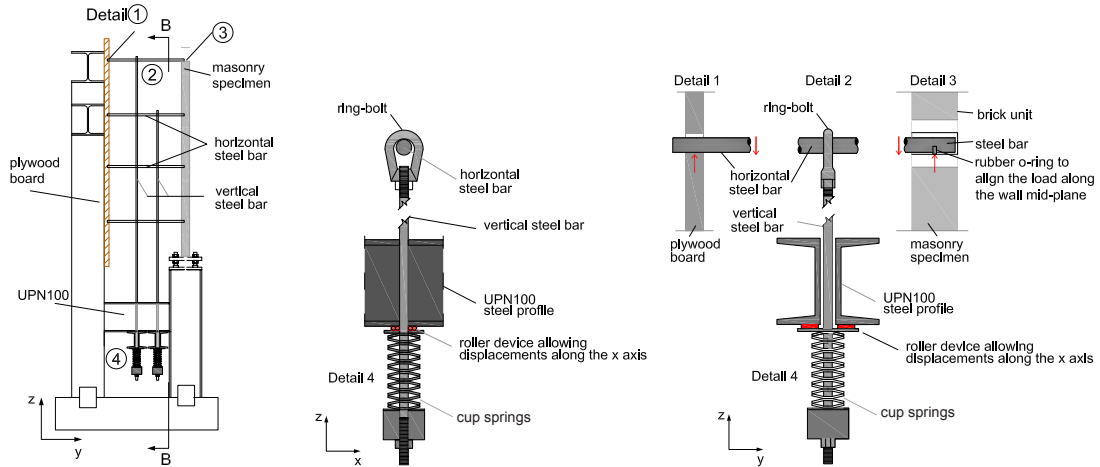
FIG. 5: Loading system

shortening. Due to the reduced stiffness, the spring shortening made possible applying very small loading variations. The regular monitoring of the springs displacements during the application of the settlements enabled the recovery of their load when necessary, and therefore to maintain the façade pre-load constant. Further details on the design of the loading system can be found in Giardina et al. (2012).

Settlement application

In Test 1, differential settlements were applied in cascade to the two left end columns of the dry block structure subjected to its self weight only, with no pre-load. The settlement of the left end column was imposed by lowering the supporting plate in 18 steps of 0.42 mm, reaching a final displacement of 7.5 mm on the scaled model; this would correspond to a settlement of 150 mm on the full scale structure. In the second part of the same test, a vertical displacement of 7.5 mm was gradually imposed to the second column from the left.

In Test 2, after applying the amplified load, a total settlement of 8.8 mm was applied to the left end column of the dry block model in 21 steps of 0.42 mm. This corresponds to a total settlement of 176 mm on the full scale structure. For all settlement scenarios, the magnitude of the applied displacements is consistent with the possible subsidence of the soil underneath the prototype, based on the field investigation reported in Section 2.

The model was then dismounted and reassembled by adding thin mortar layers in between the original masonry blocks, and Test 3 was performed on the new model. A progressive settlement of 8.8 mm was initially applied to the left end column of the model, followed by the displacement of the second column, up to 13.4 mm. In all tests, the deformation of the cup springs was periodically monitored to guarantee a constant value of pre-load of the façade.

7

Monitoring system

A photogrammetric system was used to monitor the absolute and relative displacements of the masonry blocks as a function of the progressively applied settlements. To correct the distortion of the measurements, the position of the experimental set-up was monitored through a topographic survey system: a theodolite was used to measure the location of a grid of markers glued to the structure and the frame. The photogrammetric measurements were compared with the displacements measured by mechanical dial gauges placed in the points a, b and c of Figure 3.

EXPERIMENTAL RESULTS

This section describes the results of the three tests performed on the façade model.

Test on dry block model with no amplified loading – Test 1

The crack pattern development as a function of the increasing settlement is illustrated in Figure 6a-c. The first crack initiated at the façade top (Fig. 6a) and extended in the vertical direction towards the second column from the left (Fig. 6b). For increasing values of applied settlement new cracks developed from the upper right corner of the left window and at the crown of the arch below (Fig. 6c).

Another crack developed from the lower right corner of the left window; this crack extended to the top of the second left column, creating a compressive strut that held the portion of the structure located on the left side of the window (Fig. 6b,c).

Figure 7 shows the relation between the applied settlements and the crack width of the most relevant cracks. The trend of the curve is essentially linear, suggesting a rigid body motion of the portions of façade defined by these cracks: the stress redistribution caused by the settlement application remained constant during the first part of the test. The stress redistribution led to a new equilibrium state: no fall or partial detachment of bricks were observed up to 7.5 mm of applied settlement.

Aim of the second part of the test was to evaluate the effect of adjacent column settlements. Figure 6d shows an almost complete closure of the cracks induced by the settlement of the first column and a subsequent development of a new crack pattern. The new crack pattern is qualitatively comparable to the previous one, but its location appears as shifted to the right by one span.

Test on dry block model with amplified loading – Test 2

The second test was performed on the scaled model subjected to amplified loads, as described in Section 3. As a consequence of left end column settlement, some blocks showed visible displacements already at an initial stage of the test. The vertical component of these displacements tends to reduce the stress level inside the vertical bars controlling the pre-load. In order to guarantee a constant value of pre-load during the test, the initial deformation of the cup springs was

8

(a) v_1= 3.3 mm

(b) v_1= 5 mm

(c) v_1= 7.5 mm
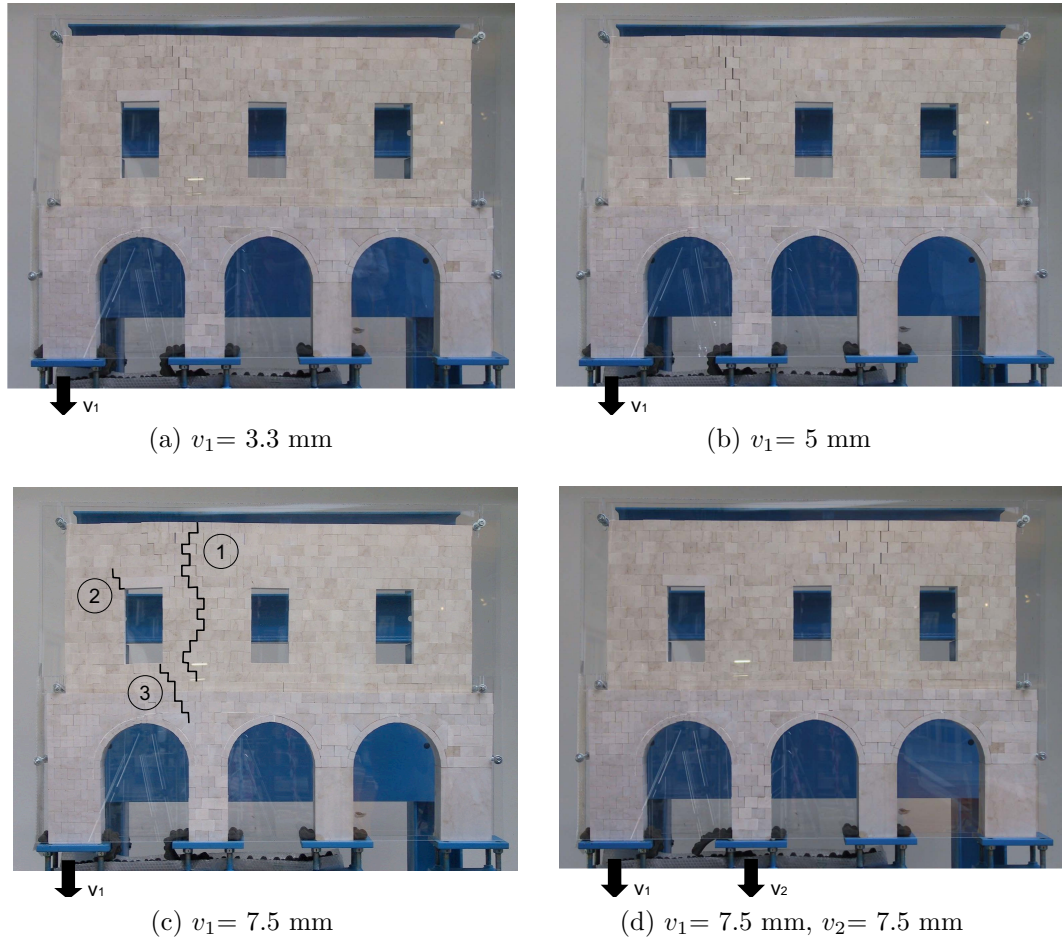
(d) v_1= 7.5 mm, v_2= 7.5 mm

FIG. 6: Test 1: Crack width evolution, façade without mortar, test with no amplified loading.

recovered after each step of applied settlement. More specifically, the recalibration was performed for each vertical bar that showed a load loss larger than 10% of the initial load. At the final applied settlement of 8.8 mm the high concentration of compressive stresses at the intrados of the left arch caused the ejection of a marble fragment.

Figures 8a-c show the crack pattern development in the last phase of the test. The damage was localised in three areas on the left side of the façade (Fig. 8d-f): above the window (crack 1), between the window and the second column from the left (crack 2) and in the left end column, at the arch spring level (crack 3). Figure 8d shows the detail of the large crack arising from the façade top. This crack significantly opens only after a relatively high value of applied displacement ($v_1 > 4.2$ mm). The location of the crack onset is affected by the load distribution device, which confines the blocks underneath it. Figure 8e shows the crack developing from the lower corner of the window. The crack
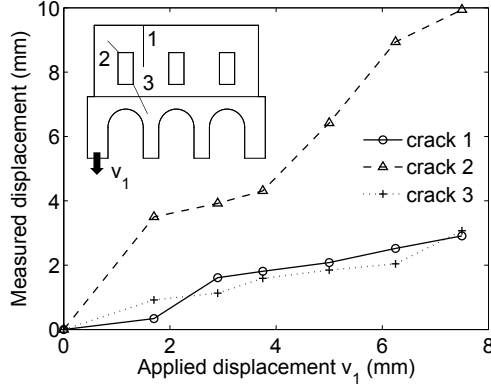
FIG. 7: Test 1: Crack pattern evolution, façade without mortar, test with no amplified loading.

is well defined and grew at an angle of approximately 60° with the horizontal direction.

Figure 9 illustrates the relation between the applied displacement and the crack width progression of the principal cracks. The curve corresponding to the crack at the façade top exhibits an initial negative slope; this was due to the initial perturbation caused by the applied displacement and resulting in a compaction of the blocks in the horizontal direction. After the first three steps of settlement application, the curve shows a change of slope, which becomes positive; this indicates the crack onset. Around the eighth step of settlement, the curve slope increases, indicating an increase in the crack opening rate. This slope, approximately linear, remains constant until the end of the test, when the crack width was about a half of the applied settlement. Figure 9 also shows the horizontal displacement measured by the mechanical dial gauge c. This displacement was mainly due to the opening of the crack onsetting at the left end column at the arch spring level. This crack was relatively small and its opening rate, almost linear, was lower than the one of the crack measured by the dial gauges a-b.

Test on mortar joint model with amplified loading – Test 3

The crack pattern development is shown in Figure 10. When the applied settlement of the left column reached 1.7 mm, crack 1 arose at the top of the structure due to the bending of the façade upper part. Almost at the same time, crack 2 onset from the lower side of the left window, defining a compressive strut acting towards the second column from the left. At 2.5 mm of displacement the increased shear stresses in the horizontal joints caused the onset of crack number 3: the mortar joints provided enough tensile strength to activate the cantilever resistant mechanism in the portion of masonry above the left end column. This behaviour is substantially different from the one exhibited by the dry block model, where the same portion of masonry, lacking any tensile strength, was gradually leaning on the settling column. Note that the location of crack 3 was likely to

10

(a) v_1= 5 mm   (b) v_1= 7.5 mm

(c) v_1= 8.75 mm   (d) crack 1, de-(e) crack 2, detail(f) crack 3, detail tail

FIG. 8: Test 2: Crack pattern evolution, façade without mortar, test with amplified loading.
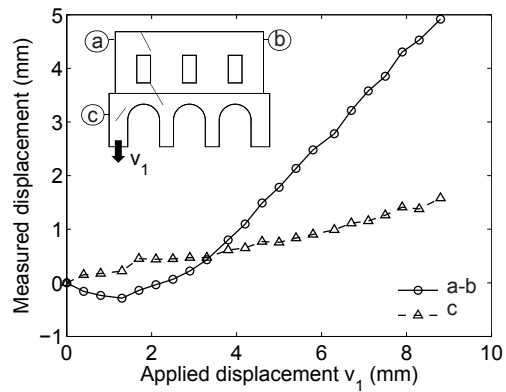
FIG. 9: Test 2: Monitored displacements, façade without mortar, test with amplified loading.

11

(a) v_1= 5 mm

(b) v_1= 7.5 mm

(c) v_1= 8.8 mm

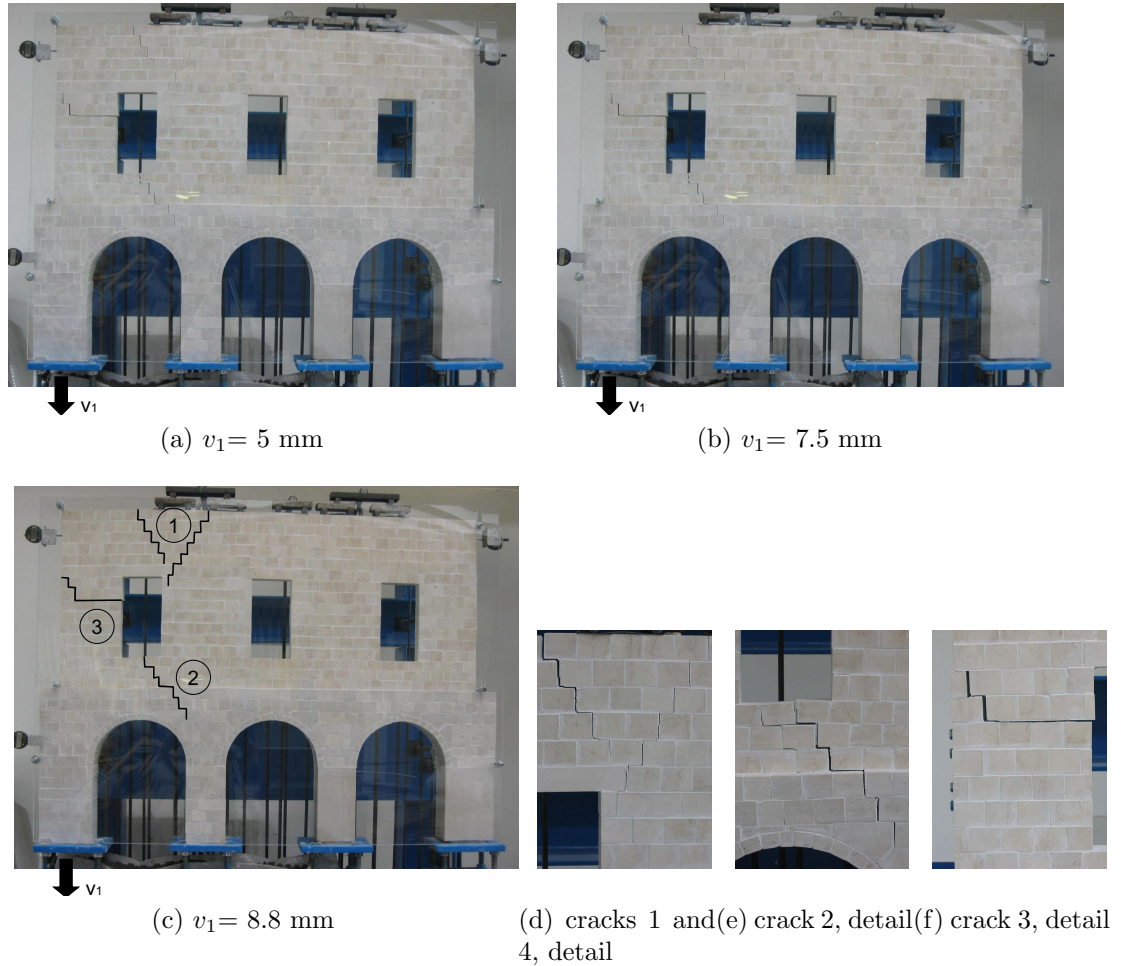(d) cracks 1 and (e) crack 2, detail (f) crack 3, detail
4, detail

FIG. 10: Test 3: Crack pattern evolution, façade with mortar, test with amplified
loading: settlement of the left end column.

have been influenced by the position of one of the vertical load application bar
(Figure 11a). By increasing the applied settlement, the weight of the cantilever
previously formed above the left window produced tensile stresses larger than the
mortar strength; this caused the onset of crack 4. The mechanism was strongly
influenced by the lintel above the window; the lintel acted as a hinge for the new
cantilever, which was completely disconnected from the structure underneath it.
In fact, Figure 11b shows that removing the lowest left block from the cantilever
did not cause any further vertical displacement. The device distributing the roof
load played a key role in this new equilibrium state by confining the portion of
masonry adjacent to the new cantilever and therefore acting as a restraint on the
cantilever rotation (Fig. 11c).

Figure 12 shows the experimental relation between the imposed settlement and
the horizontal displacements of the monitoring points. The solid line represents
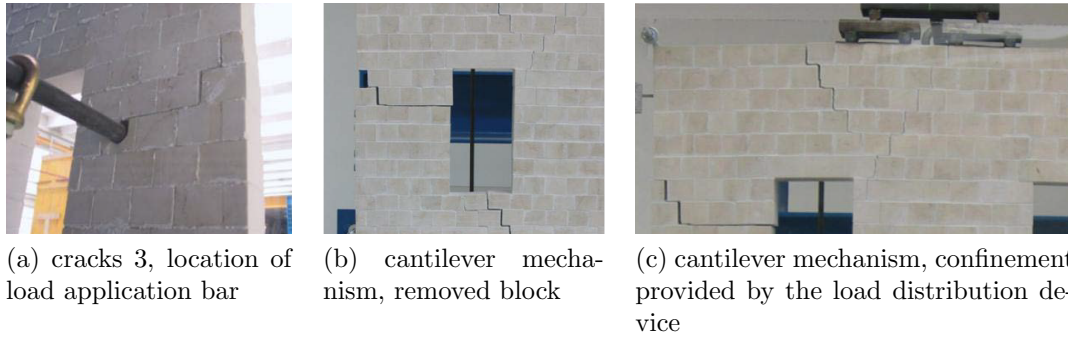
(a) cracks 3, location of load application bar

(b) cantilever mechanism, removed block

(c) cantilever mechanism, confinement provided by the load distribution device

FIG. 11: Test 3: Crack pattern details, façade with mortar, test with amplified loading: settlement of the left end column.
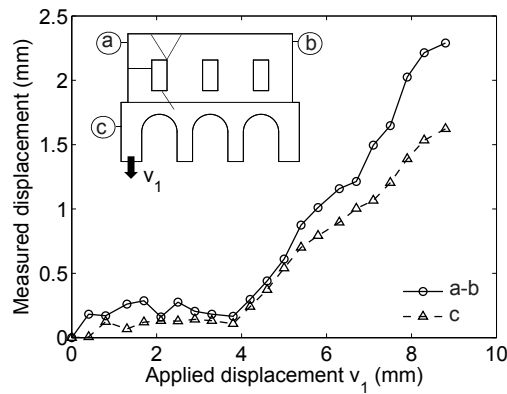

FIG. 12: Monitored displacements, façade with mortar, test with amplified loading: settlement of the left end column.

the relative displacement of the points a and b, which is the sum of crack widths 1 and 4, while the dotted line describes the absolute horizontal displacement of point c, which represents the sum of the crack width 1 and the slipping component of crack 3. The curves show an initial branch with high stiffness, as long as the stresses of the structure remain lower than the maximum strength of the mortar joints; then, the deformations increase, reaching a value of 2.3 mm for the relative displacement measured between the point a and b, and 1.6 mm at point c. Note that in this case the mechanical gauges did not capture the full displacements: the direct measurement of the final cracks width revealed for the sum of crack width 1 and 4 an opening of 2.95 mm.

The global crack pattern at the finale stage (applied settlement of 8.8 mm to the first left column) shows the macro mechanical decomposition of the structure into three blocks. The first one, delimited by the cracks 2 and 3, first settled and then rotated in an anticlockwise direction to follow the imposed displacements; the second block, confined between the cracks 3 and 4, rotated in an anticlockwise

(a) v_1= 8.8 mm   (b) v_1= 8.8 mm, v_2= 8.8 mm   (c) v_1= 8.8 mm, v_2= 13.4 mm
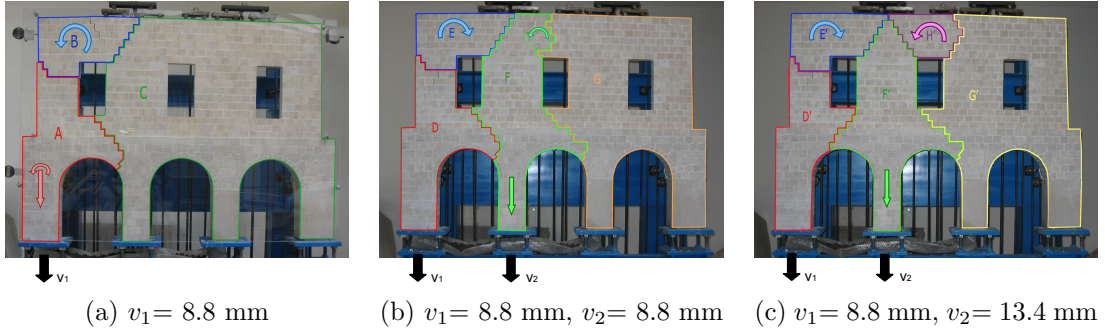
FIG. 13: Mechanisms, façade with mortar, test with amplified loading

direction, following the vertical movement of the first block, while the third block, represented by the rest of the façade, remained fixed. A further displacement of the second column, up to 13.4 mm, led to a further development of this mechanism. The progressive failure mechanisms which developed during this third tests are summarised in Figure 13.

NUMERICAL ANALYSIS

The experimental tests allowed to evaluate the prototype behaviour and offered useful information on the response of similar structures to differential settlements. Computational analyses were performed on finite element models of the specimen with mortar joints and amplified loads. Discrete and continuum crack models were used to simulate the material behaviour.

Discrete model

The discrete model enables an interpretation of the damage location in the mortar layers, because it represents the different behaviour of both the bricks and mortar layer; it offers a more reliable simulation of the crack pattern and a direct calculation of the crack width, which can be easily decomposed into slipping motion and displacement normal to the interface. However, apart from academic case studies, the discrete approach is not suitable for large scale structures, because of the need to include in the mesh the real masonry fabric and a single interface element for each mortar joint makes its preparation excessively time consuming.

In the discrete approach, the masonry is subdivided into two components: continuum elastic plane stress elements representing the bricks and non-linear interface elements describing the combination of the mortar joints and the contact surfaces between the bricks and the mortar (Figure 14a). A Coulomb friction criterion was adopted for the mortar joints. If the tensile traction t_n normal to the interface exceeds the value of f_t, a gap arises and the tensile traction is reduced to zero. The values assumed for the interface parameters are given in Table 1. Appendix A describes the shear tests that were performed on brick couplets to obtain the frictional parameters.
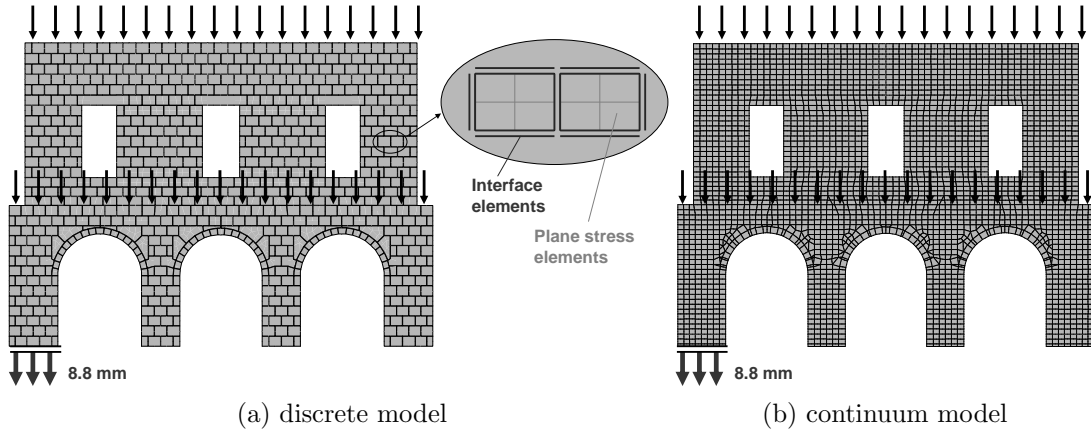
14

(a) discrete model   (b) continuum model

FIG. 14: Meshes and loading conditions.

TABLE 1: Parameters for the discrete model.

Unit brick	Young's modulus	E_u	4×10^3	N/mm^2
	Poisson's ratio	ν	0.2	
	Density	ρ	2.7×10^{-6}	kg/mm^3
Interface	Normal stiffness	k_n	2×10^2	N/mm^3
	Shear stiffness	k_s	1×10^2	N/mm^3
	Tensile strength	f_t	0.5	N/mm^2
	Cohesion	c	0.06	N/mm^2
	Friction angle	ϕ	24	∘
	Dilatancy angle	ψ	0	∘

Continuum model

In practice, the continuum model represents a more convenient approach. In this study the total strain rotating crack model was considered, which defines a unique material behaviour in terms of stress–strain relation and distributes the localised damage over a certain crack bandwidth h of the finite elements. Compared to the discrete model, an increased overall tensile strength was assumed, to account for the lack of a physical interface between bricks and joints in the continuum model. The stress–strain relationship, evaluated in the principal directions of the strain vectors, is elastic in compression and linear softening in tension, where the post-peak behaviour is described by a linear diagram governed by the fracture energy (Rots, 1997). The linear softening approach was considered as an adequate idealisation of the softening curve, in the absence of a more detailed experimental characterisation of the post-peak material behaviour. The mesh used in the continuum model is shown in Figure 14b and the values assumed for the homogenised parameters are listed in Table 2.

TABLE 2: Parameters for the continuum model.

Masonry	Young's modulus	E_u	4×10^3	N/mm^2
	Poisson's ratio	ν	0.2	
	Density	ρ	2.7×10^{-6}	kg/mm^3
	Tensile strength	f_t	0.6	N/mm^2
	Fracture energy	G_f	0.1	N/mm

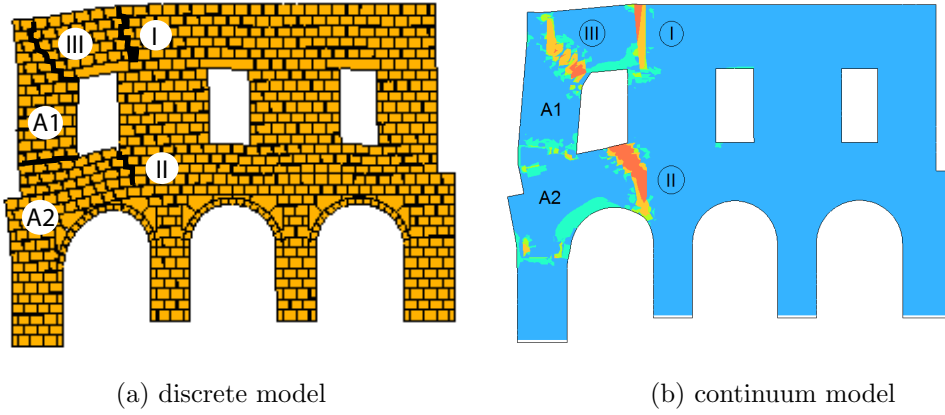(a) discrete model   (b) continuum model

FIG. 15: Crack pattern, façade with mortar, test with amplified loading: settlement of the left end column. Magnification factor = 10.

NUMERICAL RESULTS

The numerical analyses apply the discrete and total strain models to the experimental test. The results are compared in Figures 15 and 16. The crack pattern of both the models after the application of 8.8 mm of settlement to the left column (Fig. 15) shows a good agreement with the experimental test. In particular, the models are able to reproduce the localisation and propagation of cracks I, II and III, which define the rotating blocks A and B (see Fig. 13a). In both numerical models crack III starts developing at the upper corner of the left window and therefore defines a slightly different shape for the rotating block B. Furthermore, two cracking areas localised at the lower side of the window and at the spring of the arch underneath it, dividing the rotating block A in 2 portions. Note that the horizontal displacement of point c, which in the experiment quantifies the rotation of block A, for both numerical models is measured at half height of the block A2, therefore 100 mm higher than in the experiment.

Figure 16 compares the numerical and experimental results in terms of horizontal displacements of the monitored points. Both the models can reproduce the order of magnitude of total crack width that was experimentally observed.
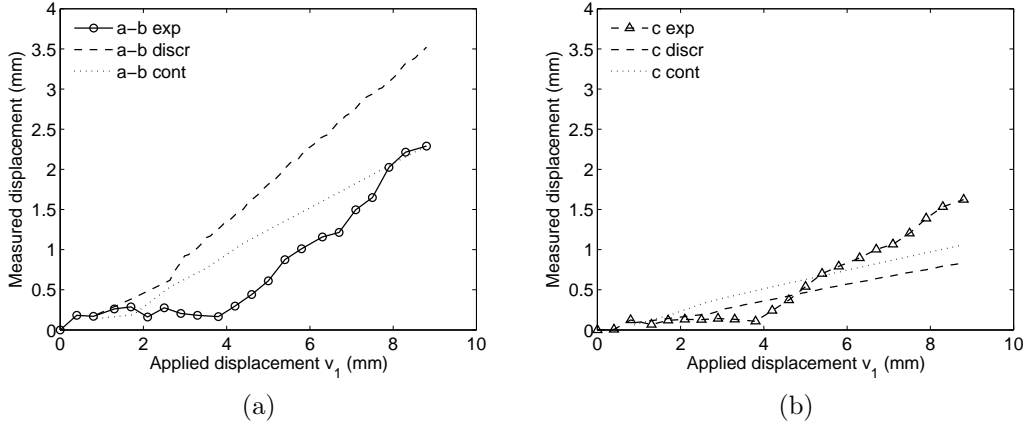
16

FIG. 16: Monitored displacements (a) a-b and (b) c, façade with mortar, test with amplified loading: settlement of the left end column.

DISCUSSION

The impact of pre-load and masonry joints on the settlement-induced damage pattern can be evaluated by comparing the results from the three experimental tests.

In the test performed on the dry block model with no amplified loading, after the development of the main vertical crack the portion of masonry above the left end column gradually leaned on the column underneath it. This movement was due to the absence of tensile strength of the masonry joints and to the lack of confinement of the façade, two conditions that prevented the development of a cantilever resistant mechanism. The gradual settlement of this portion of masonry acted as a restraint on the crack width increment of the left window crack: the weight of the masonry limited the relative slipping between the blocks. Even after the full development of the final crack pattern, and despite significant deformations, the arch was subjected to compressive stresses that were sufficient to avoid the falling of its voussoirs.

A similar deformation mechanism developed within the dry block model with amplified loading, with the major difference of a reduced (i.e. less than a half) crack width for an equal magnitude of settlement applied to the left end column (compare Figs. 6 and 8). As a further difference, in the dry block model with amplified loading, the crack arising At the lower corner of the window highlights the development of a compressive strut where the stresses caused by the upper masonry portion and transmitted by the arch concentrated.

A different damage pattern was observed in the mortar joint model with amplified loading. Here the mortar joints provided enough tensile strength to activate the cantilever resistant mechanism in the portion of masonry above the left end column. This behaviour is substantially different from the one exhibited by the dry block models, where the same portion of masonry, lacking any tensile

17

strength, was gradually leaning on the settling column. In all three models, and for both the left end columns, the differential settlements did not affect the global stability of the structure, due to a new equilibrium state induced by the stress redistribution.

This stress redistribution was correctly simulated by the numerical model, which was able to capture the crack pattern development and the crack growth with increasing applied settlements. While it is possible to conclude that both the discrete and the numerical model are suitable to the interpretation of failure mechanisms arising from different settlement scenarios, the continuum model offers the advantage of a greater flexibility for the simulation of large structure and complex geometries.

CONCLUSIONS

Experimental testing on scaled models offers a unique insight of structural problems and provides essential data for the validation of numerical predictive models. In the test presented in this work, a 1/20th scaled model of a stone masonry façade was subjected to differential settlements of its base columns. The paper described the modelling choices and experimental set-up, with particular focus on the load amplification system that enabled to reproduce the real stress conditions of the prototype. Results were presented in terms of deformations, damage pattern, crack propagation and interpretation of the failure mechanisms.

The tests performed on a model with dry joints showed that a differential settlement of the corner column would result in a severe damage of the façade. The subsiding column also moved horizontally of about 1/6 of the applied settlement, and the induced damage pattern showed a maximum crack width of approximately 1/2 of the applied settlement. However, the entire structure was able to reach a new equilibrium configuration, with localised failures but avoiding a global collapse. In the test with mortar joints, more closely reproducing the full scale structure behaviour, the tensile strength offered by the mortar, although limited, allowed for a partial redistribution of the stresses. The development of several rigid blocks, defined by the main cracks, enabled a new equilibrium configuration with a reduced amount of damage.

The results of the last experiment were used as a validation of a finite element model that simulates the nonlinear response of the façade using discrete and continuum crack models for the masonry. Both the adopted continuum and discrete finite element models can simulate the response to settlements of masonry façades, which are the most vulnerable components of historic buildings. Therefore, they can be used to predict the expected level of damage for similar buildings subject to degradation of pile foundations. Furthermore, they can be adopted in the preliminary design stage of urban underground projects, to evaluate the risk of excavation-induced damage to surface structures.

Sandrini, Norman Rossini and Benedetta Capoferri for their contribution to the experimental testing.

REFERENCES

Amorosi, A., Boldini, D., De Felice, G., Malena, M., and Sebastianelli, M. (2014). "Tunnelling-induced deformation and damage on historical masonry structures." *Geotechnique*, 64(2), 118–130.

Bettiol, G., Ceccato, F., Pigouni, A. E., Modena, C., and Simonini, P. (2016). "Effect on the structure in elevation of wood deterioration on small-pile foundation: Numerical analyses." *International Journal of Architectural Heritage*, 10(1), 44–54.

Boonpichetvong, M. and Rots, J. G. (2005). "Settlement damage of masonry buildings in soft-ground tunnelling." *Structural Engineer*, 83(1), 32–37.

Boscardin, M. D. and Cording, E. J. (1989). "Building response to excavation-induced settlement." *Journal of Geotechnical Engineering*, 115(1), 1–21.

Buckingham, E. (1914). "On physically similar systems; illustrations of the use of dimensional equations." *The Physical Review*, 4, 345–376.

Burd, H. J., Houlsby, G. T., Augarde, C. E., and G, L. (2000). "Modelling tunnelling-induced settlement of masonry buildings." *Proc Inst Civil Eng: Geotech Eng*, 143(1), 17–29.

Burland, J. B. (1995). "Assessment of risk of damage to buildings due to tunneling and excavation." *Proceedings of the 1st International Conference on Earthquake Geotechnical Engineering, IS, Tokyo, Japan*, K. Ishihara, ed., A. A. Balkema, 1189–1201.

Burland, J. B., Broms, B. B., and de Mello, V. F. B. (1977). "Behaviour of foundations and structures." *Proc. 9th Int. Conf. Soil Mech. and Found. Eng.*, Vol. 2, 495–546.

Burland, J. B., Standing, J. R., and Jardine, F. M. (2001). *Building response to tunnelling: case studies from construction of the Jubilee Line Extension, London*. CIRIA Special Publication Series. Thomas Telford, London.

Burland, J. B. and Wroth, C. P. (1974). "Settlement of buildings and associated damage." *Proceedings of Conference on Settlement of Structures*, Cambridge, Pentech Press, 611–654.

Clausen, C. A. (2010). *Biodeterioration of wood Centennial*. U.S. Dept. of Agriculture, Forest Service, Forest Products Laboratory, GTR-190. Madison, WI, Chapter 14, 14.1–14.16.

Cominelli, S., Giuriani, E., and Marini, A. (2017). "Mechanisms governing the compressive strength of unconfined and confined rubble stone masonry." *Materials and Structures*, 50(1), 10.

Dalgic, K. D., Hendriks, M. A., Ilki, A., and Broere, W. (2018a). "A two-stage numerical analysis approach for the assessment of the settlement response of the pre-damaged historic hoca pasha mosque." *International Journal of Architectural Heritage*, 0(0), 1–21.

Dalgic, K. D., Hendriks, M. A. N., and Ilki, A. (2018b). "Building response to tunnelling- and excavation-induced ground movements: using transfer functions to review the limiting tensile strain method." *Structure and Infrastructure Engineering*, 14(6), 766–779.

D'Ayala, D. (2013). "Assessing the seismic vulnerability of masonry buildings." *Handbook of Seismic Risk Analysis and Management of Civil Infrastructure Systems*, Woodhead Publishing.

de Vent, I. (2016). "Tremors and sinkholes: unforeseen effects of mining in the netherlands." *Structural Analysis of Historical Constructions - Anamnesis, diagnosis, theraphy, controls*, Taylor and F. Group, eds., 457–464.

DeJong, M. J., Hendriks, M. A. N., and Rots, J. G. (2008). "Sequentially linear analysis of fracture under non-proportional loading." *Engineering Fracture Mechanics*, 75(18), 5042–5056.

Franza, A. and Marshall, A. M. (2018). "Centrifuge modeling study of the response of piled structures to tunneling." *Journal of Geotechnical and Geoenvironmental Engineering*, 144(2).

Franzius, J. N., Potts, D. M., Addenbrooke, T. I., and Burland, J. B. (2004). "The influence of building weight on tunnelling-induced ground and building deformation." *Soil Foundation*, 44(1), 25–38.

Franzius, J. N., Potts, D. M., and Burland, J. B. (2006a). "The response of surface structures to tunnel construction." *Proc Inst Civil Eng: Geotech Eng*, 159(1), 3–17.

Franzius, J. N., Potts, D. M., and Burland, J. B. (2006b). "Twist behaviour of buildings due to tunnel induced ground movement." *Proceedings of the 5th International Conference on Geotechnical Aspects of Underground Construction in Soft Ground*, E. Kwast, K. Bakker, W. Broere, and A. Bezuijen, eds., Amsterdam, Taylor and Francis, 107–113.

Giardina, G. (2013). "Modelling of settlement induced building damage." Ph.D. thesis, Delft University of Technology, Delft.

Giardina, G., DeJong, M. J., and Mair, R. J. (2015a). "Interaction between surface structures and tunnelling in sand: Centrifuge and computational modelling." *Tunnelling and Underground Space Technology*, 50, 465–478.

Giardina, G., Graaf, A. v. d., Hendriks, M. A. N., Rots, J. G., and Marini, A. (2013). "Numerical analysis of a masonry façade subject to tunnelling-induced settlement." *Engineering Structures*, 54, 234–247.

Giardina, G., Hendriks, M. A. N., and Rots, J. G. (2010). "Numerical analysis of tunnelling effects on masonry buildings: the influence of tunnel location on damage assessment." *Advanced Materials Research*, 133, 289–294.

Giardina, G., Hendriks, M. A. N., and Rots, J. G. (2015b). "Damage functions for the vulnerability assessment of masonry buildings subjected to tunnelling." *Journal of Structural Engineering*, 141(9).

Giardina, G., Hendriks, M. A. N., and Rots, J. G. (2015c). "Sensitivity study on tunnelling induced damage to a masonry façade." *Engineering Structures*, 89, 111–129.

Giardina, G., Marini, A., Hendriks, M. A. N., Rots, J. G., Rizzardini, F., and Giuriani, E. (2012). "Experimental analysis of a masonry façade subject to tunnelling-induced settlement." *Engineering Structures*, 45, 421–434.

Goh, K. H. and Mair, R. J. (2011). "Building damage assessment for deep excavations in Singapore and the influence of building stiffness." *Geotechnical Engineering Journal of the SEAGS and AGSSEA*, 42(3).

Jacobsz, S. W., Standing, J. S., and Mair, R. J. (2006). "The influence of tunnelling on adjacent piled foundations." *Tunnelling and Underground Space Technology*, 21(3-4), 430.

Klaassen, R. K. and Creemers, J. G. (2012). "Wooden foundation piles and its underestimated relevance for cultural heritage." *Journal of Cultural Heritage*, 13(3, Supplement), S123 – S128 Wood Science for Conservation.

Korff, M. and Mair, R. J. (2013). "Response of piled buildings to deep excavations in soft soil." *18th International Conference on Soil Mechanics and Geotechnical Engineering Paris*, 2035–2038.

Laefer, D. F., Hong, L. T., Erkal, A., Long, J. H., and Cording, E. J. (2011). "Manufacturing, assembly, and testing of scaled, historic masonry for one-gravity, pseudo-static, soil-structure experiments." *Construction and Building Materials*, 25(12), 4362–4373.

Liu, G., Houlsby, G. T., and Augarde, C. E. (2000). "2-dimensional analysis of settlement damage to masonry buildings caused by tunnelling." *Structural Engineer*, 79(1), 19–25.

Losacco, N., Burghignoli, A., and Callisto, L. (2014). "Uncoupled evaluation of the structural damage induced by tunnelling." 64, 646–656(10).

Mair, R. J., Taylor, R. N., and Burland, J. B. (1996). "Prediction of ground movements and assessment of risk of building damage due to bored tunnelling." *Geotechnical Aspects of Underground Construction in Soft Ground. Proceedings of the International Symposium*, R. J. Mair and R. N. Taylor, eds., Rotterdam, Balkema, 713–718.

Meli, R. and Sanchez-Ramirez, A. R. (1997). "Rehabilitation of the Mexico City Cathedral." *Structural Engineering International*, 7(2), 101–106.

New, B. M. (1990). "Ground vibration caused by construction works." *Tunnelling and Underground Space Technology*, 5(3), 179 – 190.

Nghiem, H. L., Al Heib, M., and Emeriault, F. (2014). "Physical model for damage prediction in structures due to underground excavations." *Tunneling and Underground Construction*, 155–164.

Ovando-Shelley, E., Ossa, A., and Romo, M. P. (2007). "The sinking of Mexico City: Its effects on soil properties and seismic response." *Soil Dynamics and Earthquake Engineering*, 27(4), 333 – 343.

Pickhaver, J. A., Burd, H. J., and Houlsby, G. T. (2010). "An equivalent beam method to model masonry buildings in 3D finite element analysis." *Computers & Structures*, 88(19-20), 1049–1063.

Potts, D. M. and Addenbrooke, T. I. (1997). "A structure's influence on tunnelling-induced ground movements." *Proceedings of the Institution of Civil Engineers: Geotechnical Engineering*, 125(2), 109–125.

Rampello, S., Callisto, L., Viggiani, G., and Soccodato, F. M. (2012). "Evaluating the effects of tunnelling on historical buildings: the example of a new subway in Rome / Auswertung der Auswirkungen des Tunnelbaus auf historische Gebäude am Beispiel einer neuen U-Bahnlinie in Rom." *Geomechanics and Tunnelling*, 5(3), 275–299.

Ritter, S., DeJong, M., J., Giardina, G., and Mair, R., J. (2017a). "Influence of building characteristics on tunnelling-induced ground movements." *Geotechnique*.

Ritter, S., Giardina, G., DeJong, M., J., and Mair, R., J. (2017b). "Centrifuge modelling of building response to tunnel excavation." *International Journal of Physical Modelling in Geotechnics*.

Rots, J. (1997). *Structural masonry: an experimental/numerical basis for practical design rules*. CUR Report Series. Balkema.

Son, M. and Cording, E. J. (2005). "Estimation of building damage due to excavation-induced ground movements." *Journal of Geotechnical and Geoenvironmental Engineering*, 131(2), 162–177.

Son, M. and Cording, E. J. (2007). "Evaluation of building stiffness for building response analysis to excavation-induced ground movements." *Journal of Geotechnical and Geoenvironmental Engineering*, 133(8), 995–1002.

UNIBS (1999). "Prime valutazioni sulla situazione delle fondazioni del palazzo della loggia." *Report no.*, Centro di studio e ricerca per la conservazione ed il recupero dei beni architettonici ed ambientali, University of Brescia, Brescia (April). (in Italian).

van de Kuilen, J.-W. G. (2007). "Service life modelling of timber structures." *Materials and Structures*, 40(1), 151–161.

APPENDIX A. SHEAR TEST

Shear tests were performed o block couplets with an interposed bed joint for varying vertical confinement, thus simulating masonry shear behaviour under different compression levels. Compressive stress levels were selected to reproduce the masonry stress magnitude at the first floor level (1 N/mm^2), near to the roof (0.1 N/mm^2) and at an intermediate confinement level of 0.5 N/mm^2.

The masonry specimens were brick couplets bonded by thin 1 mm lime mortar joint. Figure 17a,b shows the special testing equipment designed for scaled masonry shear testing. The tests were carried out in displacement control. By tightening bolt A, a relative displacement was applied to steel profiles B and C, which were glued to the bottom and top brick respectively. The alignment of the steel components B an C allowed applying the shear load along the mortar bed-joint mid plane. A roller support was interposed between the masonry couplet top face and the transverse steel plate to avoid any friction during the test. Vertical rebar pretension allowed applying the confinement stress distribution to the specimen. In order to keep the vertical stress level constant throughout the test, the vertical rebar stiffness was significantly reduced by means of a series of conical spring washers. This way no significant variation in the applied vertical load was induced by the bar deformation caused by the joint slip. Figure 18a shows average shear stress vs displacement curves for varying vertical confinement levels. All curves show an initial linear elastic branch until the shear peak strength is reached, when a crack develops and propagates along the brick to mortar joint interface. Peak shear strength increases for increasing vertical confinement. The post peak shows a softening trend until pure friction resistance is reached. For increasing applied displacement a slight reduction in the friction resistance follows the wearing of the fracture asperities. As expected, the failure behaviour of masonry joints under shear actions for varying moderate vertical confinement levels, can be described by the Mohr Coulomb friction law (Figure 18b):
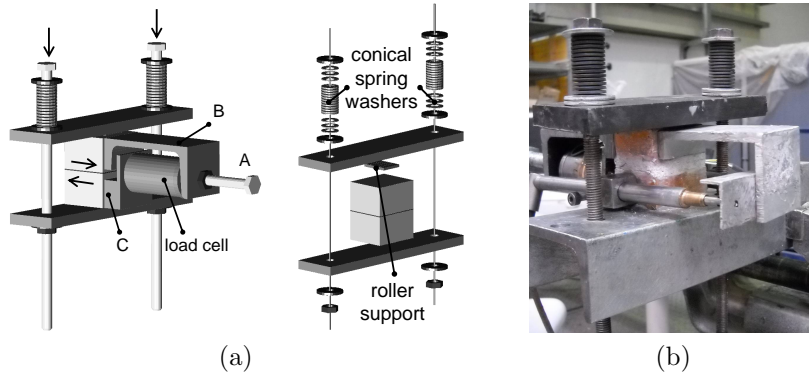
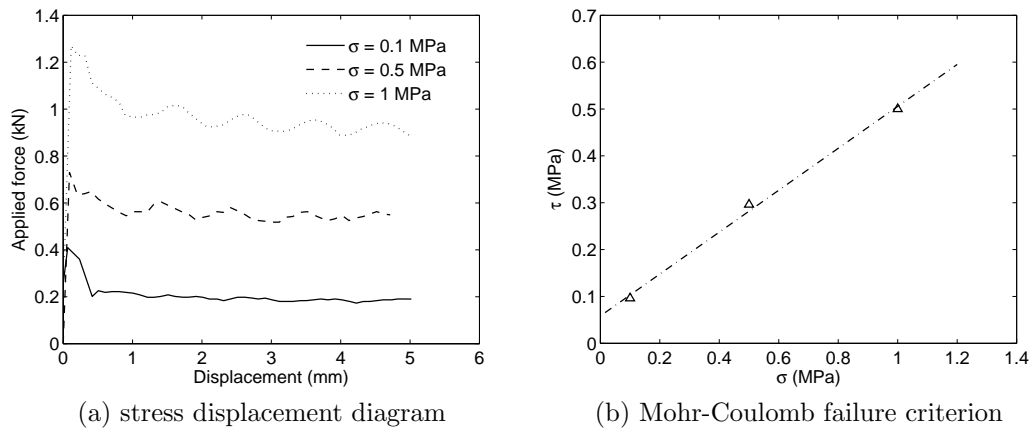FIG. 17: a) Shear test set-up; b) masonry couplet subjected to shear test.

(a) stress displacement diagram

(b) Mohr-Coulomb failure criterion

FIG. 18: Shear test results.

$$\tau_u = c - \sigma \tan \phi = 0.06 + 0.45\sigma$$

where c is the initial shear strength, $\tan \phi$ is the tangent of the friction angle of the interface between brick unit and mortar joint and σ is the vertical confinement. Mechanical properties are in line with those presented by Cominelli et al. (2017). For higher normal compressive stresses, the validity of the Coulomb law is lost and crushing/shearing of the units is observed.